

# Model Selection and Inference in Variational Longitudinal Distributed Lag Models for Analyzing Post-flight Effects of In-flight Exposures

Mark J. Meyer \*

Department of Mathematics and Statistics,  
Georgetown University

and

Selina Carter

Department of Statistics and Data Science,  
Carnegie Mellon University

and

Eileen McNeely

Department of Environmental Health,  
Harvard T. H. Chan School of Public Health

and

Elizabeth J. Malloy

Department of Mathematics and Statistics,  
American University

August 25, 2022

## Abstract

Flight-related health effects are a growing area of environmental health research with most work examining the concurrent impact of in-flight exposure on cardiac health. One understudied area is on the post-flight effects of in-flight exposures. Studies investigating the health effects of flight often collect a range of repeatedly sampled, time-varying exposure-related measurements under both crossover and longitudinal sampling designs. A natural choice to model the relationship between these

---

\*Funding for the motivating data in this work was provided by the U.S. Federal Aviation Administration (FAA) Office of Aerospace Medicine through the National Air Transportation Center of Excellence for Airliner Cabin Environment Research (ACER)/Research in the RITE, Cooperative Agreements 10-C-RITE-HU, 07-C-RITE-HU, and 04-C-ACE-HU.

lagged exposures and post-flight outcomes is the distributed lag model (DLM). However, longitudinal DLMs are a lightly studied area. Thus, we propose a class of models for analyzing longitudinal DLMs where the random effects can incorporate more general structures—including random lags—that arise from repeatedly sampling lagged exposures. We develop variational Bayesian algorithms to estimate model components under differing random effect structures, derive a novel variational AIC for model selection between these structures, and show the converged variational estimates can be used to test for the difference between two semiparametric curves under the crossover design. We then analyze the impact of in-flight, lagged exposure-related physiological effects on post-flight heart health. We also perform simulation studies to evaluate the operating characteristics of our models and inference procedures.

*Keywords:* variational Bayesian inference, longitudinal data analysis, variational AIC, global test of differences, flight-induced cardiac health effects

# 1 Introduction

Research on the concurrent and post-flight effects of in-flight exposures to altitude is an understudied, but burgeoning area of work in environmental health. Studies on the impact of altitude on heart health have found that arrhythmic events can occur during transitions to and from cruising altitude and appear to have age-related differences [Behn et al., 2014]. These cardiac health effects also occur during flight conditions as Oliveira-Silva et al. [2016] demonstrate, with altered cardiovascular functioning persisting in participants up to 24 hours after commercial flight. Chatterjee et al. [2021] examine cardiac arrests during air travel both in-flight and post-flight, finding that rapid intervention is essential. In a controlled setting, Meyer et al. [2019] describe the results of a crossover experiment where participants were exposed to flight conditions in a hypobaric chamber. Those authors found significant, concurrent increases in heart rate and heart rate variability over the duration of the flight when compared to control. Despite these findings, little work has been done to examine the lagged effects of exposure to altitude, and its related physiological changes, on post-flight heart health.

Lagged, exposure-related physiological effects during flight may take on different forms. One such effect is blood oxygen saturation ( $\text{SaO}_2$ ) which naturally fluctuates over time but is also impacted by flight conditions. Specifically, desaturation, where  $\text{SaO}_2$  falls below 90%, occurs when at altitude [Meyer et al., 2019]. This altitude exposure-related effect may have a deleterious impact on post-flight cardiac health as measured by heart rate and heart rate variability. In-flight  $\text{SaO}_2$  was collected as part of the chamber study described by Meyer et al. [2019] every five minutes over the duration of a six-hour simulated flight, but not analyzed; nor was its relationship with post-flight heart-health metrics explored. A natural choice of model for analyzing this relationship is the distributed lag model which

relates lagged effects of an exposure variable to an outcome taken after the exposure occurs.

Distributed lag models or DLMs have a large body of literature regarding their formulation and estimation. We briefly review a limited selection of this literature. DLMs may be unconstrained, where each lag has its own effect in a model, or constrained, where some transformation has been performed to reduce the parameter space [Zanobetti et al., 2000]. For example, with regards to the penalization of correlated lagged effects, Welty et al. [2009] consider penalized splines for a constrained DLM. Chen et al. [2018] employ ridge-type shrinkage to compare unconstrained DLMs to constrained DLMs while Chen et al. [2019] consider interactions of multiple pollutants. Liu et al. [2018] use a novel group and fused lasso penalty along with kernel regression to analyze multi-pollutant mixtures. Wilson et al. [2017] use principal component bases to constrain lagged effects for identifying windows of susceptibility that may interact with different covariates.

Other authors consider various types of clustered effects in DLMs. For instance, Chang et al. [2015] cluster hazards by week in a hierarchical time-to-event DLM. Liu et al. [2017] examine spatial-temporal models with lagged effects of pollution exposure. For binary outcomes, Warren et al. [2020b] develop a model that estimates subject-specific main effects that vary both by spatial location and by time. From the epidemiology literature, Baek et al. [2016] explore hierarchical DLMs to analyze associations between the built environment and health with spatial effects. In the context of a case-control design, Warren et al. [2020a] build spatial models to identify critical windows of susceptibility to exposure. While these clustered and hierarchical models often incorporate random intercepts (or their equivalence), none examine the case where lagged effects vary by subject. However, in the case of the chamber study, some of the lagged in-flight exposures may be subject-specific, indicating a need for a new class of DLMs.

In this manuscript, we propose a modeling framework for longitudinal distributed lag models or LDLMs. Our models can accommodate subject-specific, or random, effects that can potentially arise from more complex structures when lagged exposures are longitudinally sampled, including under the crossover experimental design. We employ penalized B-splines to estimate lagged effects and to model random lags. To further reduce the computational burden, we conduct estimation using variational Bayesian inference. This necessitates the development of model selection tools for variational LDLMs as it is common practice in longitudinal analyses to select the random effect structure before considering the mean model [Fitzmaurice et al., 2011]. Thus, we derive variational AICs (VAICs) for our LDLMs and explore decision rules for model selection. We show in simulation that model selection using VAICs performs well in identifying the correct model and that our models have good properties in terms of bias and mean integrated squared error (MISE).

For inference, we investigate two interval construction procedures, point-wise intervals and simultaneous bands, as well as a global test of the difference in two curves. Work by You et al. [2014], Wang and Blei [2019], and Zhang and Zhou [2020] establishes some Frequentist properties of variational methods. We extend this literature by showing that the LDLM variational algorithm admits a form of the estimated mean that is well-suited for use in a Frequentist global test of differences. We investigate its properties in simulation for the difference in curves from the crossover design.

The motivation for this work comes from Meyer et al. [2019], a hypobaric chamber study examining the impact of exposure to altitude on cardiac health using a crossover design. While Meyer et al. [2019] study the concurrent in-flight effects, the post-flight effects of in-flight exposures have not been analyzed. To our knowledge, no previous studies have assessed the impact of lagged  $\text{SaO}_2$  on post-flight heart health. We investigate these effects

using the full LDLM framework on two outcomes of interest taken post-flight: heart rate and root Mean Squared Standard Deviations of N-N intervals (rMSSD), a measure of heart rate variability. We examine the impact of exposure to flight on  $\text{SaO}_2$ 's lagged relationship with heart health both in the full data and in a subgroup analysis of pre-specified groups.

The remainder of this manuscript is organized as follows: Section 2 describes our motivating data in detail. In Section 3, we establish our framework for estimating LDLMs, conducting model selection, and performing inference. Section 4 details our simulation study where we assess the model discrimination of the VAIC and the Frequentist characteristics of our inference procedures. In Section 5, we present our analysis of the chamber study data. Finally, we provide a discussion of our work in Section 6.

## 2 Motivating Data

Motivation for the LDLM comes from a crossover design study examining the impact of exposure to altitude during flight on concurrent heart health metrics [Meyer et al., 2019]. As part of the study, participants entered a hypobaric pressure chamber outfitted with airplane seats on two separate days. On one day, the chamber's air pressure was depressurized to the equivalent of 7,000 ft altitude, below the 8,000 ft common in commercial flight [McNeely et al., 2011]. We refer to this as the "flight day" and consider it the active treatment. On the other day, the air pressure in the chamber remained the same as outside, near sea level. This day is the "control day." The order in which participants received the treatment was block randomized depending on their calendar dates in the chamber.

During each day, participant  $\text{SaO}_2$  was monitored every five minutes for the duration of the simulated flight (or control), approximately six hours. Post-flight measurements of heart health were also monitored including heart rate and heart rate variability as measured

by rMSSD. In the original study, Meyer et al. [2019] found that concurrent exposure to altitude had a significant impact on heart rate and rMSSD. The authors use experimental condition as a proxy in their analysis for physiological changes induced by altitude exposure. Our current goal is to see if lagged SaO<sub>2</sub> impacts the first five-minute measurement taken immediately after flight (or control). SaO<sub>2</sub> is a physiological feature that is affected by altitude and as such varies both within and between days, flight vs. control, with each participant serving as their own control. Additional variables of interest include an experiment effect to control for the order in which the treatments occurred and the time of day the participant entered the chamber which can impact autonomic responses.

In total, there were 26 participants available for analysis. Three subgroups were identified a priori, related to the relative health of the participants. All participants were over the age of 55 and categorized as being healthy (11 participants), smokers (6), or those with diagnosed cardiovascular disease (9). These groups are the focus of our secondary, subgroup analysis. All participants provided informed written consent. Protocols for the study were approved by the Human Subjects Committees at the Harvard School of Public Health (Institutional Review Board Protocol #P15170-101), the Civilian Aerospace Medical Institute, and the University of Oklahoma Medical Center.

## 3 Statistical Methods

### 3.1 Variational Bayesian Inference

We begin with a brief description of variational Bayesian inference. Let  $\boldsymbol{\theta}$  be a vector of parameters and  $\mathbf{Y}$  denote a vector of observed data. The posterior distribution for  $\boldsymbol{\theta}$  given  $\mathbf{Y}$  is  $p(\boldsymbol{\theta}|\mathbf{Y}) = p(\mathbf{Y}, \boldsymbol{\theta})/p(\mathbf{Y})$ . Typically,  $p(\mathbf{Y})$  is intractable and posterior estimates

need to be obtained algorithmically. For the arbitrary density  $q$ ,  $p(\mathbf{Y})$  is bounded below by  $\underline{p}(\mathbf{Y}; q)$  where  $\underline{p}(\mathbf{Y}; q) = \exp \left[ \int q(\boldsymbol{\theta}) \log \left\{ \frac{p(\mathbf{Y}, \boldsymbol{\theta})}{q(\boldsymbol{\theta})} \right\} d\boldsymbol{\theta} \right]$ . Variational algorithms work by maximizing  $\underline{p}(\mathbf{Y}; q)$  over a class of densities,  $q$ , that are tractable. This in turn minimizes the Kullback-Leibler Divergence between  $q(\boldsymbol{\theta})$  and the posterior,  $p(\boldsymbol{\theta}|\mathbf{Y})$ .

Given a partition of  $\boldsymbol{\theta}$  into  $M$  subcomponents,  $\{\boldsymbol{\theta}_1, \dots, \boldsymbol{\theta}_M\}$ , we use the mean field variational Bayesian approximation to construct  $q(\boldsymbol{\theta})$ , specifically  $q(\boldsymbol{\theta}) = \prod_{m=1}^M q_m(\boldsymbol{\theta}_m)$ . This approach approximates the posterior as the product of these  $q$ -densities which are analogous to conditional posterior densities resulting from a Gibbs sampler [Gelman et al., 2013]. Optimal densities are obtained iteratively with convergence, and therefore minimization, occurring when changes in the variation lower bound,  $\underline{p}(\mathbf{Y}; q)$ , become negligible. For a thorough introduction to variational Bayesian techniques with examples, see Ormerod and Wand [2010] and Blei et al. [2017].

### 3.2 Variational Longitudinal DLMS

Let  $Y_{ij}$  denote the  $j$ th response of the  $i$ th subject. We define the following models:

$$Y_{ij} = \mathbf{x}'_{ij}\boldsymbol{\beta} + \mathbf{l}'_{ij}\boldsymbol{\gamma}_j + \mathbf{l}'_{ij}\mathbf{g}_i + \varepsilon_{ij} \text{ (random lag) and} \quad (1)$$

$$Y_{ij} = \mathbf{x}'_{ij}\boldsymbol{\beta} + \mathbf{l}'_{ij}\boldsymbol{\gamma}_j + b_i + \varepsilon_{ij} \text{ (random intercept)} \quad (2)$$

where  $\mathbf{g}_i$  and  $b_i$  are the random lag and random intercept. The fixed effects,  $\mathbf{x}_{ij}$ , and lagged effects,  $\mathbf{l}_{ij}$ , are  $1 \times P$  and  $1 \times \ell$  with corresponding vectors of coefficients  $\boldsymbol{\beta}$  and  $\boldsymbol{\gamma}_j$ . The lagged effects may vary by  $j$  for the case where each subject receives both treatments under a crossover design, giving each treatment its own estimated effect. The target of inference under the crossover design is the difference curve,  $\boldsymbol{\delta} = \boldsymbol{\gamma}_1 - \boldsymbol{\gamma}_0$  where  $j = 0$  denotes the lagged effects under a control and  $j = 1$  denotes a treatment. For the longitudinal case, we drop the  $j$  index,  $\boldsymbol{\gamma}_j = \boldsymbol{\gamma}$ . We assume  $\varepsilon_{ij} \stackrel{iid}{\sim} N(0, \sigma^2)$  for both models.



To reduce the number of parameters that need to be estimated and to model the functional form of the distributed lag, we fit a constrained DLM using a basis expansion of the lagged effects. Suppose  $\Theta$  is the  $\ell \times K$  matrix of known basis functions. The basis expanded coefficients are  $\gamma_j = \Theta\gamma_j^S$  (for the crossover model),  $\gamma = \Theta\gamma^S$  (longitudinal model), and  $\mathbf{g}_i = \Theta\mathbf{g}_i^S$  for some selection of knots,  $K$ —the basis expansions do not necessarily have to have the same number of knots. Under the crossover design, the basis-space versions of equations (1) and (2) are

$$Y_{ij} = \mathbf{x}'_{ij}\boldsymbol{\beta} + \mathbf{l}'_{ij}\Theta\boldsymbol{\gamma}_j^S + \mathbf{l}'_{ij}\Theta\mathbf{g}_i^S + \varepsilon_{ij} \text{ (random lag) and} \quad (3)$$

$$Y_{ij} = \mathbf{x}'_{ij}\boldsymbol{\beta} + \mathbf{l}'_{ij}\Theta\boldsymbol{\gamma}_j^S + b_i + \varepsilon_{ij} \text{ (random intercept).} \quad (4)$$

When the data arises from a longitudinal design,  $\boldsymbol{\gamma}_j^S = \boldsymbol{\gamma}^S$ .

For both the fixed and random lag components, we implement penalized B-splines using the mixed model representation. Thus,  $\Theta$  is a matrix of B-spline basis functions of a size dependent upon the number of knots selected and the number of lags. The general penalty matrix,  $\mathcal{P} = \xi D_0 + (1 - \xi)D_2$ , is weighted between the zeroth derivative matrix ( $D_0$ ) and the second derivative matrix ( $D_2$ ). The parameter  $\xi$  controls the desired tradeoff between shrinkage and smoothness, with values near 0 favoring shrinkage. The penalty priors on  $\boldsymbol{\gamma}_j^S$  and  $\boldsymbol{\gamma}^S$  are  $\boldsymbol{\gamma}_j^S \sim N(\mathbf{0}, \lambda_j \mathcal{P}_j^{-1})$  and  $\boldsymbol{\gamma}^S \sim N(\mathbf{0}, \lambda_\gamma \mathcal{P}_\gamma^{-1})$ , where  $\lambda_j$  and  $\lambda_\gamma$  are tuning-parameters for corresponding penalty matrices,  $\mathcal{P}_j$  and  $\mathcal{P}_\gamma$ —both of form  $\mathcal{P}$ . We select a small number of knots, setting  $K_j = 8$  for  $j = 0, 1$  or  $K_\gamma = 8$  and set  $\xi = 0.01$ .

The prior on the random lag,  $\mathbf{g}_i^S$ , is  $\mathbf{g}_i^S \stackrel{iid}{\sim} N[\mathbf{0}, \lambda_g \mathcal{P}_g^{-1}]$  where  $\lambda_g$  is a tuning-parameter. The penalty matrix,  $\mathcal{P}_g$ , also has the same form as  $\mathcal{P}$  with dimension depending on the choice of  $K_g$ . We select  $K_g = n$ , where  $n$  is the total number of subjects. This choice results in one knot for each subject which effectively reduces the random lag dimension, in the transformed space, to a single subject-specific parameter. Subject-specific lags are still

estimated after transformation but since our model generates estimates in the transformed space, this knot selection provides a large dimension reduction while maintaining separate parameters for each subject.

Regardless of the model, we place weakly informative priors on the components of  $\boldsymbol{\beta}$ ,  $\beta_p \stackrel{iid}{\sim} N(0, \sigma_b^2)$  with  $\sigma_b^2$  fixed at something large. For the random intercept model, the vector  $\mathbf{b}$  consists of the  $b_i$  which are independent normals,  $b_i \stackrel{iid}{\sim} N(0, \sigma_u^2)$ . We place inverse-gamma priors (and hyper-priors) on all variance components:  $\sigma^2 \sim IG(a_e, b_e)$ ,  $\lambda_j \sim IG(a_j, b_j)$  or  $\lambda_\gamma \sim IG(a_\gamma, b_\gamma)$ , and  $\sigma_u^2 \sim IG(a_u, b_u)$  or  $\lambda_g \sim IG(a_g, b_g)$ , depending on the model. The hyper-parameters for each variance prior are set to something small, 0.01 for example.

Using a mean field variational Bayesian approximation, we obtain approximation densities or  $q$ -densities for each component of the spline-based models in equations (3) and (4). We let  $\boldsymbol{\theta}$  generically denote the coefficients which vary by model and design. The random lag model has  $\boldsymbol{\theta} = [ \boldsymbol{\beta} \quad \boldsymbol{\gamma}^S \quad \mathbf{g}^S ]$  (longitudinal) or  $\boldsymbol{\theta} = [ \boldsymbol{\beta} \quad \boldsymbol{\gamma}_0^S \quad \boldsymbol{\gamma}_1^S \quad \mathbf{g}^S ]$  (crossover) for all transformed subject-specific lag effects  $\mathbf{g}^S$ . In general, the  $q$ -densities are then  $q(\boldsymbol{\theta}) \sim N \left[ \boldsymbol{\mu}_{q(\boldsymbol{\theta})}, \boldsymbol{\Sigma}_{q(\boldsymbol{\theta})} \right]$ ,  $q(\sigma^2) \sim IG \left[ a_e + \frac{N}{2}, B_{q(\sigma^2)} \right]$ ,  $q(\lambda_j) \sim IG \left[ a_j + \frac{K_j}{2}, B_{q(\lambda_j)} \right]$ , and  $q(\lambda_g) \sim IG \left[ a_g + \frac{K_g}{2}, B_{q(\lambda_g)} \right]$ , where the  $j$  can take on 0 or 1 (indicating crossover treatments) or  $\gamma$  (longitudinal). The subscript- $q(\cdot)$  notation indicates the parameter to which the quantity belongs under the mean field approximation. For the random intercept model,  $\mathbf{g}^S$  is replaced with  $\mathbf{b}$ ,  $a_g$  with  $a_u$ ,  $b_g$  with  $b_u$ ,  $K_g$  with  $K_u$ , and  $\lambda_g$  with  $\sigma_u^2$ . The specific values for the quantities  $\boldsymbol{\mu}_{q(\boldsymbol{\theta})}$ ,  $\boldsymbol{\Sigma}_{q(\boldsymbol{\theta})}$ ,  $B_{q(\sigma^2)}$ ,  $B_{q(\lambda_0)}$ ,  $B_{q(\lambda_1)}$ , and  $B_{q(\lambda_g)}$  are in Algorithm 1.

The forms of the design matrix referenced in Algorithm 1,  $\mathbf{C}$ , and the stacked vector of outcomes,  $\mathbf{Y}$ , are defined as follows: let  $\mathbf{Y}$  be a  $(\sum_{i=1}^n m_i) \times 1$  vector where  $m_i$  denotes the number of measurements per subject  $i$ ,  $\mathbf{X}$  be a  $(\sum_{i=1}^n m_i) \times P$  matrix for  $P$  fixed effects, and  $\mathbf{U}$  be a  $\sum_{i=1}^n m_i \times n$  block diagonal matrix. The main lagged effects matrix  $\mathbf{L}$  is a

block diagonal  $(\sum_{i=1}^n m_i) \times 2\ell$  matrix under the crossover design and  $(\sum_{i=1}^n m_i) \times \ell$  under the longitudinal design. The random lag design matrix  $\mathbf{W} = \text{diag}\{\mathbf{L}_i\}$  is a block diagonal matrix with blocks consisting of the subject-specific matrices  $\mathbf{L}_i$  formed by stacking the  $\mathbf{l}_{ij}$ . Thus,  $\mathbf{W}$  has dimension  $(\sum_{i=1}^n m_i) \times \ell n$ . In the case of the crossover design, as in the chamber study,  $m_i = 2 \forall i$  and the full design matrix is  $\mathbf{C} = [\mathbf{X} \mathbf{L}(\mathbf{I}_2 \otimes \Theta) \mathbf{W}(\mathbf{I}_n \otimes \Theta)]$  for the random distributed lag and  $\mathbf{C} = [\mathbf{X} \mathbf{L}(\mathbf{I}_2 \otimes \Theta) \mathbf{U}]$  for the random intercept. The design matrices simplify under the longitudinal case to  $\mathbf{C} = [\mathbf{X} \mathbf{L}\Theta \mathbf{W}(\mathbf{I}_n \otimes \Theta)]$  (random lag) or  $\mathbf{C} = [\mathbf{X} \mathbf{L}\Theta \mathbf{U}]$  (random intercept).

Algorithm 1 iterates until changes in the variational lower bound become minimal. The log of this lower bound for the crossover random lag model is

$$\begin{aligned} \log[\underline{p}(\mathbf{Y}; q)] &= \frac{1}{2}(P + K_0 + K_1 + K_g) - \frac{N}{2} \log(2\pi) - \frac{P}{2} \log(\sigma_b^2) \\ &+ \frac{1}{2} \log(|\Sigma_q(\boldsymbol{\theta})|) - \frac{1}{2\sigma_b^2} \left[ \boldsymbol{\mu}_q(\boldsymbol{\beta})' \boldsymbol{\mu}_q(\boldsymbol{\beta}) + \text{tr} \left\{ \Sigma_q(\boldsymbol{\beta}) \right\} \right] \\ &- a_e \log(b_e) - \left( a_e + \frac{N}{2} \right) \log(B_{q(\sigma^2)}) + \log \left( \Gamma \left( a_e + \frac{N}{2} \right) \right) - \log(\Gamma(a_e)) \\ &+ a_0 \log(b_0) - \left( a_0 + \frac{K_0}{2} \right) \log(B_{q(\lambda_0)}) + \log \left( \Gamma \left( a_0 + \frac{K_0}{2} \right) \right) - \log(\Gamma(a_0)) \\ &+ a_1 \log(b_1) - \left( a_1 + \frac{K_1}{2} \right) \log(B_{q(\lambda_1)}) + \log \left( \Gamma \left( a_1 + \frac{K_1}{2} \right) \right) - \log(\Gamma(a_1)) \\ &+ a_g \log(b_g) - \left( a_g + \frac{K_g}{2} \right) \log(B_{q(\lambda_g)}) + \log \left( \Gamma \left( a_g + \frac{K_g}{2} \right) \right) - \log(\Gamma(a_g)), \end{aligned}$$

where  $\boldsymbol{\mu}_q(\boldsymbol{\beta})$  is  $\boldsymbol{\mu}_q(\boldsymbol{\theta})$  subset to the quantities corresponding to  $\boldsymbol{\beta}$ , likewise for  $\Sigma_q(\boldsymbol{\beta})$ . For the random intercept model, the last line replaces with  $a_g$  with  $a_u$ ,  $b_g$  with  $b_u$ ,  $K_g$  with  $K_u$ , and  $\lambda_g$  with  $\sigma_u^2$ . The lower bound for the longitudinal design omits the fifth line. Code to implement all algorithms in R is available at <https://github.com/markjmeyer/LDLM>.

### 3.3 Model Selection Criterion

You et al. [2014] propose a variational AIC (VAIC) for multiple linear regression. In that

context, they show that the VAIC has good asymptotic properties and converges in probability to the standard AIC. The general form of their VAIC is  $VAIC \equiv -2 \log p(\mathbf{Y}|\boldsymbol{\theta}^*) + 2P_D^*$ , where  $\boldsymbol{\theta}^* = E_q(\boldsymbol{\theta})$  and  $P_D^* = 2 \log p(\mathbf{Y}|\boldsymbol{\theta}^*) - 2E_q[\log p(\mathbf{Y}|\boldsymbol{\theta})]$ . The expectation is taken with respect to the variational approximation densities, i.e. the  $q$ -densities. We derive  $\log p(\mathbf{Y}|\boldsymbol{\theta}^*)$  and  $E_q[\log p(\mathbf{Y}|\boldsymbol{\theta})]$  for the LDLM to obtain

$$\begin{aligned} \log p(\mathbf{Y}|\boldsymbol{\theta}^*) &= -\frac{N}{2} \log(2\pi) - \frac{N}{2} \left[ \log \{B_{q(\sigma^2)}\} - \log \left( a_e + \frac{N}{2} - 1 \right) \right] \\ &\quad - \frac{1}{2} \frac{a_e + \frac{N}{2} - 1}{B_{q(\sigma^2)}} \left\{ \mathbf{Y} - \mathbf{C}\boldsymbol{\mu}_{q(\boldsymbol{\theta})} \right\}' \left\{ \mathbf{Y} - \mathbf{C}\boldsymbol{\mu}_{q(\boldsymbol{\theta})} \right\} \text{ and} \\ E_q[\log p(y|\boldsymbol{\theta})] &= -\frac{N}{2} \log(2\pi) + \frac{N}{2} \left[ \psi \left( a_e + \frac{N}{2} \right) - \log \{B_{q(\sigma^2)}\} \right] \\ &\quad - \frac{1}{2} \frac{a_e + \frac{N}{2}}{B_{q(\sigma^2)}} \left[ \text{tr} \left\{ \mathbf{C}\boldsymbol{\Sigma}_{q(\boldsymbol{\theta})}\mathbf{C}' \right\} + \left\{ \mathbf{Y} - \mathbf{C}\boldsymbol{\mu}_{q(\boldsymbol{\theta})} \right\}' \left\{ \mathbf{Y} - \mathbf{C}\boldsymbol{\mu}_{q(\boldsymbol{\theta})} \right\} \right], \end{aligned}$$

where  $\psi(\cdot)$  denotes the digamma function and  $\boldsymbol{\theta}$  depends on model specification. Combining, the VAIC for the LDLM is then

$$\begin{aligned} VAIC &= N \log \left( a_e + \frac{N}{2} - 1 \right) + N \log(2\pi) - 2N\psi \left( a_e + \frac{N}{2} \right) + N \log \{B_{q(\sigma^2)}\} \\ &\quad + 2 \frac{a_e + \frac{N}{2}}{B_{q(\sigma^2)}} \text{tr} \left\{ \mathbf{C}\boldsymbol{\Sigma}_{q(\boldsymbol{\theta})}\mathbf{C}' \right\} + \frac{a_e + \frac{N}{2} + 1}{B_{q(\sigma^2)}} \left\{ \mathbf{Y} - \mathbf{C}\boldsymbol{\mu}_{q(\boldsymbol{\theta})} \right\}' \left\{ \mathbf{Y} - \mathbf{C}\boldsymbol{\mu}_{q(\boldsymbol{\theta})} \right\}. \end{aligned}$$

This formulation applies to both the random intercept and random lag models where  $\boldsymbol{\Sigma}_{q(\boldsymbol{\theta})}$  and  $\boldsymbol{\mu}_{q(\boldsymbol{\theta})}$  are the values from Algorithm 1 upon convergence and will depend on the model. Because the theoretical results in You et al. [2014] were derived for non-longitudinal models, we empirically examine the properties of the VAIC we derive for use in selecting the structure of the random effects in LDLMs.

As with the standard AIC, the smallest VAIC often suggests the best model fit. We refer to this as the minimum decision rule. Parsimonious models are, however, also desirable when model fits are similar. Thus other rules might impose a threshold on the absolute difference in VAICs between two candidate models. When the difference is under

the threshold, the more parsimonious model (i.e., the random intercept model) would be selected. We examine the minimum decision rule along with absolute difference thresholds of varying tolerances in our simulation study.

### 3.4 Interval Estimation for Crossover Design

The tendency of variational algorithms to underestimate the variance of mean model components, even when the means themselves are unbiased and consistent, is well documented [Gelman et al., 2013]. Any inferential developments must take this into consideration and thoroughly investigate the properties of intervals derived from variational Bayesian estimation. Since our motivating data comes from a crossover design study, we focus on the construction of intervals for the difference in treatment-specific curves,  $\boldsymbol{\delta} = \boldsymbol{\gamma}_1 - \boldsymbol{\gamma}_0$ .

We explore two different interval constructions for  $\boldsymbol{\delta}$ : a point-wise interval using the variational estimates and a simultaneous band, as described by Ruppert et al. [2003]. For the point-wise intervals, we construct the variance for each element of  $\boldsymbol{\delta}$ ,  $\delta(t)$ , in the usual fashion:  $Var[\delta(t)] = Var[\gamma_1(t)] + Var[\gamma_0(t)] - 2Cov[\gamma_1(t), \gamma_0(t)]$  with variances and covariances estimated using the corresponding components of  $\boldsymbol{\Sigma}_q(\boldsymbol{\theta})$  at convergence. Since the  $q$ -densities for both  $\boldsymbol{\gamma}_0$  and  $\boldsymbol{\gamma}_1$  are Gaussian, the distribution of their difference is also Gaussian. Using this, and the variances for each  $\delta(t)$ , we construct an interval at each lag, separately. Combining all lag-specific intervals results in a point-wise interval for  $\boldsymbol{\delta}$ .

The point-wise intervals may not always achieve nominal coverage owing to the possible underestimation of the variance. Thus, we also construct a joint interval for  $\boldsymbol{\delta}$  using simultaneous bands. Similar to Ruppert et al. [2003], we note that

$$\begin{bmatrix} \hat{\boldsymbol{\gamma}}_0^S - \boldsymbol{\gamma}_0^S \\ \hat{\boldsymbol{\gamma}}_1^S - \boldsymbol{\gamma}_1^S \end{bmatrix} \sim N \left[ \mathbf{0}, \boldsymbol{\Sigma}_q(\boldsymbol{\gamma}_0^S, \boldsymbol{\gamma}_1^S) \right], \quad (5)$$

where  $\dot{\sim}$  denotes “approximately follows.” The  $100(1 - \alpha)\%$  simultaneous band for  $\boldsymbol{\delta}$  is  $\hat{\boldsymbol{\delta}} \pm m_{1-\alpha} \widehat{\text{SD}}(\hat{\boldsymbol{\delta}})$ , where  $\widehat{\text{SD}}(\hat{\boldsymbol{\delta}})$  is the same as in the point-wise interval. The key difference is the critical value,  $m_{1-\alpha}$ , which is the  $(1 - \alpha)$  quantile of the random variable

$$\sup_t \left| \frac{\hat{\delta}(t) - \delta}{\widehat{\text{SD}}\{\hat{\delta}(t)\}} \right| \approx \max_t \left| \frac{\hat{\delta}(t) - \delta}{\widehat{\text{SD}}\{\hat{\delta}(t)\}} \right|. \quad (6)$$

To obtain  $m_{1-\alpha}$ , we generate 10,000 samples from (5), project the samples into the data space, construct (6) for  $\delta = 0$ , and find the  $(1 - \alpha)$  quantile. The longitudinal models use these intervals as well; a description of their construction is in the Supplementary Material.

### 3.5 Global Test of Differences

Zhang et al. [2000] and Zhang and Lin [2003] discuss hypothesis testing for comparing two or more semiparametric curves. The test statistic, which we refer to as the ZLS test, requires the existence of a vector,  $\mathbf{c}(t)$ , such that the estimate of a semiparametric function,  $f(t)$ , can be written as  $\hat{f}(t) = \mathbf{c}(t)'Y$  at time  $t$ . We apply this test in the crossover design setting to construct a global test of the differences being equal to zero. Algorithm 1 admits an explicit form of the  $\mathbf{c}(t)$  vector for estimating each element of  $\boldsymbol{\delta}$ ,  $\delta(t)$ , which can be derived from the mean component,  $\boldsymbol{\mu}_q(\boldsymbol{\theta})$ .

Let  $\boldsymbol{\Sigma}_q(\boldsymbol{\gamma}_0^S)$  and  $\boldsymbol{\Sigma}_q(\boldsymbol{\gamma}_1^S)$  denote the covariance matrices that correspond to the vectors of treatment-specific effects  $\boldsymbol{\gamma}_0^S$  and  $\boldsymbol{\gamma}_1^S$ , respectively. Further, let  $\mathbf{C}_0$  and  $\mathbf{C}_1$  be matrices whose columns consist of the columns of the matrix  $\mathbf{C}$  that correspond to these treatment-specific effects. Denote the following vectors  $\boldsymbol{\eta}_0(t) = \left( \frac{a_e + \frac{N}{2}}{B_q(\sigma^2)} \right) \boldsymbol{\Sigma}_q(\boldsymbol{\gamma}_0^S) \mathbf{C}_{0,t}$  and  $\boldsymbol{\eta}_1(t) = \left( \frac{a_e + \frac{N}{2}}{B_q(\sigma^2)} \right) \boldsymbol{\Sigma}_q(\boldsymbol{\gamma}_1^S) \mathbf{C}_{1,t}$ , for the  $t$ th columns of  $\mathbf{C}_0$  and  $\mathbf{C}_1$ . Then,  $\mathbf{c}_0(t) = \boldsymbol{\eta}_0(t)\boldsymbol{\Theta}'$  and  $\mathbf{c}_1(t) = \boldsymbol{\eta}_1(t)\boldsymbol{\Theta}'$  are vectors such that  $\hat{\gamma}_0(t) = \mathbf{c}_0(t)'Y$  and  $\hat{\gamma}_1(t) = \mathbf{c}_1(t)'Y$ . This allows us to make the observation that, upon convergence of Algorithm 1,  $\mathbf{c}(t) = \mathbf{c}_1(t) - \mathbf{c}_0(t)$  is a vector such that  $\hat{\delta}(t) = \mathbf{c}(t)'Y$ . This vector forms the foundation of a global test of  $H_0 : \delta(t) = 0 \forall t$ .

The statistic for the ZLS test under the crossover design is  $G(Y) = \int_0^\ell Y' \mathbf{c}(t) \mathbf{c}(t)' Y dt = Y' \mathbf{S} Y$ , for  $\mathbf{S} = \int_0^\ell \mathbf{c}(t) \mathbf{c}(t)' dt$ . As in Zhang et al. [2000] and Zhang and Lin [2003], we approximate the distribution of  $G(Y)$  as a scaled chi-squared, using Satterthwaite [1943]. Thus, for the mean,  $\mathbf{E}$ , and variance,  $\mathbf{V}$ , of  $Y$  under  $H_0$ , the mean and variance of  $G(Y)$  are  $e = \mathbf{E}' \mathbf{S} \mathbf{E} + tr(\mathbf{S} \mathbf{V})$  and  $\psi = 2tr\{(\mathbf{S} \mathbf{V})^2\} + 4\mathbf{E}' \mathbf{S} \mathbf{V} \mathbf{S} \mathbf{E}$ . Under the null,  $\mathbf{S} \mathbf{E}$  is negligible, so these quantities are frequently approximated with  $e \approx tr(\mathbf{S} \mathbf{V})$  and  $\psi \approx 2tr\{(\mathbf{S} \mathbf{V})^2\}$ . Setting the approximate versions of  $e$  and  $\psi$  equal to the mean and variance of a scaled chi-squared,  $\kappa \chi_\nu^2$ , results in a scaling factor of  $\kappa = \psi/(2e)$  and a degrees of freedom of  $\nu = 2e^2/\psi$ . The  $p$ -value for the test can be approximated by finding  $Pr[\chi_\nu^2 > G(Y)/\kappa]$ .

## 4 Simulation Study

We now evaluate the LDLM framework with the goal of identifying decision rules for when the VAIC selects the “correct” model and how misspecification impacts the model’s operating characteristics. Our simulation aims to address this by varying the design between crossover and longitudinal, the sample sizes ( $n = 25$  or  $50$ ), the sampling density of the lag ( $\ell = 40$  or  $60$ ), and three true lagged effects: a peak effect, cyclical effect, and sigmoidal effect. For each combination, we generate 500 datasets under a simulated random intercept model and 500 datasets under a simulated random lag model. We apply both LDLMs to each dataset to observe how misspecification impacts absolute bias, mean integrated squared error (MISE), and interval coverage. Under the crossover design, we also examine the power and size of the ZLS test. For the power analysis, we introduce a scaling factor that varies from 1.1 to 5 by 0.1 to control the simulated difference between the groups. Tables 1 to 3 average across all simulated crossover design datasets, thus each value in those tables is calculated using 20,000 simulated datasets. The results for the size of the

ZLS test are based on 1,000 simulated datasets. Descriptions of the functions for each of the true lagged effects are in the Supplementary Material.

## 4.1 Model Selection Discrimination and Estimation

The goal of the VAIC is to select a “best” model, but “best” model varies depending on the model selection approach. We examine the accuracy of four different decision rules for selecting between the random intercept and random lag models: a minimum decision rule and absolute differences of  $< 2$ ,  $< 5$ , and  $< 10$ , representing varying tolerances in model selection. For the latter decision rules, the random intercept model is selected when the absolute differences falls below the threshold. Table 1 contains the percent of correctly specified models, by decision rule, for the crossover design when  $\ell = 60$ . Even under the strictest decision rule, the VAIC selects the correct model at least 97% of the time.

When using the absolute difference based decision rules, an approach that favors parsimonious models, the accuracy when the true model is the random intercept model increases as the threshold increases. This does not simultaneously impact accuracy when the true model is the random lag model which maintains a high percent of correctly identified models regardless of the effect, sample size, or decision rule. When the threshold is set to 10, the VAIC correctly identifies the model in excess of 99% of the time.

Table 2 presents the absolute bias and MISE for the crossover design when  $\ell = 60$ . Overall, absolute bias and MISE are lower when the true model is the random intercept model and all metrics shrink toward zero as sample size increases. When the model is correctly specified, the absolute bias and MISE are lower than when the model is incorrectly specified. However, in some cases the trade-off is minor such as when the sample size is 25 or when the true model is the random intercept model. When the sample size is 50 and



when the true model is the random lag model, the bias and MISE can be much larger if the model is incorrectly specified. Similar results for the simulation when  $\ell = 40$  are in the Supplementary Material.

## 4.2 Interval Coverage and Global Test Characteristics

Frequentist evaluations of variational methods are increasingly more common with variational models often producing ideal Frequentist properties, see for example You et al. [2014], Wang and Blei [2019], and Zhang and Zhou [2020]. We now examine the coverage of both the point-wise and simultaneous intervals for  $\delta$ . To calculate coverage, we determine whether or not the simulated effect at each time point  $t$  is contained the interval and then average over all  $\ell$  lags and all simulated datasets. The intervals used to calculate coverage in Table 3 were all constructed at the 95% level. The most notable result is that, regardless of sample size, true model, or effect, the simultaneous intervals always cover the truth. However, the point-wise intervals are often more efficient as they are closer to nominal for a number of combinations and are mostly above 90%. The point-wise intervals achieve nominal to near-nominal coverage in a number of instances seen in Table 3. Coverage of the point-wise intervals tends to be better when the model is correctly specified.

Figures 1 and 2 contain the power and size, respectively, for the ZLS test under the crossover design for  $n = 25$  and  $\ell = 60$ —a sample size and sampling density similar to our motivating data. The rows of the figures correspond to different effects while the columns correspond to different data generating models. The solid green lines are the power (or size) when the fitted model is a random lag while dashed blue lines are the power (or size) when the fitted model is the random intercept. The x-axes in Figure 1 vary by the scaling factor. Overall, as the scaling factor increases, the power of the ZLS test increases. Power

is always higher when the model is correctly specified and the test is more powerful when the random intercept model is the true model. We calculate power using an  $\alpha$  of 0.05.

The size of the ZLS test varies by the level of the test, what the true underlying model is, and whether or not the model was correctly specified. The x-axes in Figure 2 vary by the level,  $\alpha$ , and include a reference line to denote the nominal level (dotted black line). When the random intercept model is the true model, the test from the misspecified model is quite conservative. Even the correctly specified model has size below nominal for most  $\alpha$ . When the true model is the random lag model, however, the size of the test is closer to nominal—particularly when the model has been correctly specified. The ZLS test is closest to nominal when  $\alpha$  is 0.04 or lower, although even at an  $\alpha$  of 0.05 the size when the random lag model is the true model is between 0.04 and 0.05. Similar results from the simulation when  $n = 50$  and  $\ell = 40$  are in the Supplementary Material.

### 4.3 Longitudinal Design

The results for the longitudinal designs with two, three, four, and five measurements can be found in the Supplementary Material but do not differ much from the crossover design. When the data arises from any longitudinal design, the VAIC correctly identifies the model in excess of 99% of the time, regardless of the decision rule. Correctly specified models also have lower bias and MISE, though these values shrink toward zero as  $n$  increases, regardless of specification. Coverage for the point-wise interval is typically closest to nominal when the model is correctly specified and is always above nominal for the random lag models. The coverage results for the simultaneous bands are the same for the longitudinal design as seen for the crossover design. These results do not vary much with the sampling density.

## 5 Post-flight Effects of In-flight Exposure

The primary goal of our analysis is to examine the effect of lagged, exposure-induced changes in SaO<sub>2</sub> on heart rate (HR) and rMSSD, focusing first on the comparison between the two experimental conditions. Prior to analysis, rMSSD is log-transformed as is a common practice with this kind of data [Meyer et al., 2019]. All models include the non-lagged covariates indicating the order in which the conditions occurred, to control for an experimental effect, and the time of day the participant entered the chamber, to account for potential autonomic responses in the outcome. As a secondary analysis, we also consider the effects of lagged changes in SaO<sub>2</sub> on both outcomes by the pre-defined health groups: healthy participants, cardiac patients, and smokers.

### 5.1 Primary Analyses

We apply both LDLMs to the chamber study data and use the VAIC to select the random effect structure. Using the minimum rule, the VAIC selected the correct model a minimum of 97% of the time in simulation, thus we implement the minimum decision rule. Table 4 contains the resulting VAICs. For the model we select, we also perform the ZLS test to test for the difference between the lagged effect on the flight day versus the control day. The test statistic, degrees of freedom, and corresponding  $\chi^2$  p-values for these models are also in Table 4. Regardless of outcome type, the VAIC is smallest for the random intercept model, selecting it as the “best” model. For both outcomes, the ZLS test is not significant ( $p$ -values of 0.8126 and 0.9321), indicating no global difference between experimental conditions on the lagged association of SaO<sub>2</sub> with either HR or rMSSD when examining all available participants. Estimated curves from the primary models for the control and flight days as well as their difference can be found in the Supplementary Material.

Since treatment assignment does not impact the association, we next run a longitudinal model to examine the effect of lagged SaO<sub>2</sub> on HR and rMSSD. In addition to the experimental effect and time-of-day covariates, we also include in these models a non-lagged indicator for treatment: 1 for flight, 0 for control. We use the VAIC again to select between random effect structures. Based on the work of You et al. [2014], the VAIC can also be used to select between the different mean models for SaO<sub>2</sub> implied by the crossover and the longitudinal designs. The results of this modeling are also in Table 4 which suggest that the data, for either outcome, is better fit by the mean model that corresponds to the longitudinal design for SaO<sub>2</sub> with a random intercept. Because its coverage under the longitudinal design is reasonable for the random intercept model, we examine the 95% point-wise intervals in the Supplementary Material. When HR is the outcome, we find evidence of a lagged effect between 110 and 120 minutes that is significantly related to an increase in post-flight HR. This suggests a potential, delayed impact of SaO<sub>2</sub>, although the corresponding changes in HR are minimal, ranging from 1.138 to 1.439, see the Supplementary Material.

## 5.2 Subgroup Analyses

The subgroups—those with cardiovascular disease ( $n = 9$ ), smokers (6), and healthy individuals (11)—were defined prior to participant enrollment. Inclusion in the cardiac group required patients to have moderate cardiac disease, including those with coronary artery disease, a past history of severe blockage or infarction, and congestive heart failure (classified as I and II according to the New York Heart Association). The smoker group consisted of current tobacco smokers without cardiac disease. Finally, the healthy group contained participants who were non-smokers and had no reported cardiac disease. The healthy group did, however, contain patients with other chronic disease diagnoses including hypertension,

asthma, diabetes, obesity, or mental illness.

For participants within each group and for each outcome, we fit both LDLMs, perform model selection, and conduct the ZLS test. The results are in Table 5. For both outcomes in the smoker subgroup, the VAIC selects the random lag model. In the healthy group, the VAIC identifies the random lag model as the best model when HR is the outcome, although the values are close to each other: 57.59 for the random lag, 59.53 for the random intercept. In the rMSSD models for the healthy group and all of the cardiac group models, the random intercept model has the best fit, according to the VAIC.

All ZLS tests fail to find a significant difference between experimental conditions in the lagged effects of SaO<sub>2</sub>, except when the outcome is HR in the cardiac group. The unadjusted  $p$ -value is 0.016 ( $\chi^2_\nu = 8.743$ ,  $\nu = 2.09$ ). Even after adjusting for multiple comparisons within tests from HR-based subgroup models, the ZLS would reject the null since both the Bonferroni corrected and Benjamini-Hochberg corrected  $p$ -values are 0.0478. This suggests that the lagged effect of SaO<sub>2</sub> on HR in the cardiac group may differ when under exposure to altitude. Due to the small sample size, this result merely indicates a possible association which warrants further studies that are specifically designed to assess the impact of flight on compromised travelers. Graphs depicting the estimated lagged effects of SaO<sub>2</sub> on HR in the cardiac group are in the Supplementary Material.

## 6 Discussion

Additional methodological developments are required to keep up with growing analytical demand as flight health researchers continue to collect data with increasingly complex structures. This manuscript presents a full framework for the analysis of lagged effects under longitudinal and crossover designs using variational LDLMs which, to our knowledge,

represents the first work on this class of models. The framework includes the derivation of a novel model selection criterion along with inference procedures. Finally, we present an innovative application of the ZLS test, showing it can be constructed using variational estimates to test between lagged effects under differing experimental conditions.

In an extensive simulation study, we demonstrate the ability of the VAIC to select the true random effect model. The VAIC’s discrimination under both the crossover and longitudinal designs is in excess of 97% regardless of the decision rule. For that reason, we suggest using the minimum decision rule in general. The VAIC performs well in the LDLM setting because in the Bayesian modeling context, the different random effect models constitute different mean models in the Frequentist sense. Because there is no difference in how the “fixed” and “random” effects are treated in the original Bayesian model, we are ultimately selecting between different subject-specific mean models and therefore benefit from the asymptotic properties of the VAIC described by You et al. [2014].

Our simulations also demonstrate the LDLM’s operating characteristics with both bias and MISE decreasing as the sample size increases. We show that the coverage of the point-wise interval achieves or exceeds the nominal rate under a variety of combinations, regardless of the design. The ZLS test also performs well in simulation under the crossover design, attaining good power while maintaining nominal or below nominal size. These properties improve as the sample size increases as well. Importantly, our simulation illustrates the benefit of first correctly identifying the true model using the VAIC. Correctly identified models have lower bias and MSE, better coverage and size, and higher power.

The primary analysis suggests that the effect of SaO<sub>2</sub> on post-flight HR and rMSSD is not significantly altered by exposure to altitude overall, although we do find evidence of lagged effects of SaO<sub>2</sub> on HR in general from the longitudinal analysis. In the secondary

analysis, we identify a difference in the lagged effect of SaO<sub>2</sub> on HR among participants with diagnosed cardiovascular disease. Given the sample size, the finding warrants further investigation into the impact of flight on passengers with known cardiac risks. Abbasi [2022] describes evidence of an increased cardiovascular risk among patients who were previously infected with SARS-CoV-2. Identifying potential flight-related heart health problems is of particular importance as these patients resume commercial flight and as SARS-CoV-2 infections become endemic.

## SUPPLEMENTARY MATERIAL

Additional results from the simulation study and analysis are in the supplementary materials. We make the R code used to produce the simulations and all analyses described in this paper, along with the relevant datasets, available at <https://github.com/>.

## References

- J. Abbasi. The covid heart—one year after sars-cov-2 infection, patients have an array of increased cardiovascular risks. *Journal of the American Medical Association*, 327: 1113–1114, 2022.
- J. Baek, E. V. Sanchez-Vaznaugh, and B. N. Sánchez. Hierarchical distributed-lag models: Exploring varying geographic scale and magnitude in associations between the built environment and health. *American Journal of Epidemiology*, 183:583–592, 2016.
- C. Behn, G. A. Dinamarca, N. F. De Gregorio, V. Lips, E. A. Vivaldi, D. Soza, M. A. Guerra, R. F. Jiménez, E. A. Lecannelier, H. Varela, and J. A. Silva-Urra. Age-related arrhythmogenesis on ascent and descent: “autonomic conflicts” on hypoxia/reoxygenation at high altitude? *High Altitude Medicine & Biology*, 15:356–363, 2014.

- D. M. Blei, A. Kucukelbir, and J. D. McAuliffe. Variational inference: a review for statisticians. *Journal of the American Statistical Association*, 112:859–877, 2017.
- H. H. Chang, J. L. Warren, L. A. Darrow, B. J. Reich, and L. A. Waller. Assessment of critical exposure and outcome windows in time-to-event analysis with application to air pollution and preterm birth study. *Biostatistics*, 16:509–521, 2015.
- N. A. Chatterjee, K. Kume, C. Drucker, P. J. Kudenchuk, and T. D. Rea. Incidence, mechanism, and outcomes of on-plane versus off-plane cardiac arrest in air travelers. *Journal of the American Heart Association*, 10:e021360, 2021.
- Y. H. Chen, B. Mukherjee, S. D. Adar, V. J. Berrocal, and B. A. Coull. Robust distributed lag models using data adaptive shrinkage. *Biostatistics*, 19:461–478, 2018.
- Y. H. Chen, B. Mukherjee, and V. J. Berrocal. Distributed lag interaction models with two pollutants. *Journal of the Royal Statistical Society, Series C*, 68:79–97, 2019.
- G. M. Fitzmaurice, N. M. Laird, and J. H. Ware. *Applied Longitudinal Analysis*. John Wiley & Sons, Inc., Hoboken, NJ, 2<sup>nd</sup> edition, 2011.
- A. Gelman, J. B. Carlin, H. S. Stern, D. B. Dunson, A. Vehtari, and D. B. Rubin. *Bayesian Data Analysis*. Chapman and Hall-CRC, Boca Raton, FL, 3<sup>rd</sup> edition, 2013.
- S. H. Liu, J. F. Bobb, K. H. Lee, C. Gennings, C. Claus Henn, D. Bellinger, C. Austin, L. Schnaas, M. M. Tellez-Rojo, H. Hu, R. O. Wright, M. Arora, and B. A. Coull. Lagged kernel machine regression for identifying time windows of susceptibility to exposures of complex mixtures. *Biostatistics*, 19:325–341, 2018.
- Y. Liu, G. Shaddick, and J. V. Zidek. Incorporating high-dimensional exposure modelling into studies of air pollution and health. *Statistics in Biosciences*, 9:559–581, 2017.



- E. McNeely, J. D. Spengler, and J. Watson. Health effects of aircraft cabin pressure in older and vulnerable passengers. Technical Report Report No. RITE-ACER-CoE-2011-2011, Federal Aviation Administration: Airliner Cabin Environment Research, 2011.
- M. J. Meyer, I. Mordukhovich, G. A. Wellenius, M. A. Mittleman, J. P. McCracken, B. A. Coull, and E. McNeely. Changes in heart rate and rhythm during a crossover study of simulated commercial flight in older and vulnerable participants. *Frontiers Physiology*, 10:1339, 2019.
- I. Oliveira-Silva, A. S. Leicht, M. R. Moraes, H. G. Simoes, S. Del Rosso, C. Córdova, and D. A. Boulosa. Heart rate and cardiovascular responses to commercial flights: relationships with physical fitness. *Frontiers in Physiology*, 7:648, 2016.
- J. T. Ormerod and M. P. Wand. Explaining variational approximations. *The American Statistician*, 64:140–153, 2010.
- D. Ruppert, M. P. Wand, and R. J. Carroll. *Semiparametric regression*. Cambridge University Press, Cambridge, United Kingdom, 2003.
- F. E. Satterthwaite. An approximate distribution of variance components. *Biometrika*, 2: 110–114, 1943.
- Y. Wang and D. M. Blei. Frequentist consistency of variational bayes. *Journal of the American Statistical Association*, 114:1147–1161, 2019.
- J. L. Warren, W. Kong, T. J. Luben, and H. H. Chang. Critical window variable selection: estimating the impact of air pollution on very preterm birth. *Biostatistics*, 21:790–806, 2020a.

- J. L. Warren, T. J. Luben, and H. H. Chang. A spatially varying distributed lag model with application to an air pollution and term low birth weight study. *Journal of the Royal Statistical Society, Series C*, 69:681–696, 2020b.
- L. J. Welty, R. D. Peng, S. L. Zeger, and F. Dominici. Bayesian distributed lag models: Estimating effects of particulate matter air pollution on daily mortality. *Biometrics*, 65:282–291, 2009.
- A. Wilson, Y.-H. M. Chiu, H.-H. L. Hsu, R. O. Wright, R. J. Wright, and B. A. Coull. Bayesian distributed lag interaction models to identify perinatal windows of vulnerability in children’s health. *Biostatistics*, 18:537–552, 2017.
- C. You, J. T. Ormerod, and S. Müller. On variational bayes estimation and variational information criteria for linear regression models. *Australian & New Zealand Journal of Statistics*, 56:73–87, 2014.
- A. Zanobetti, M. P. Wand, J. Schwartz, and L. M. Ryan. Generalized additive distributed lag models: Quantifying mortality displacement. *Biostatistics*, 1:279–292, 2000.
- A. Y. Zhang and H. H. Zhou. Theoretical and computational guarantees of mean field variational inference for community detection. *Annals of Statistics*, 48:2575–2598, 2020.
- D. Zhang and X. Lin. Hypothesis testing in semiparametric additive mixed models. *Biostatistics*, 4:57–74, 2003.
- D. Zhang, X. Lin, and M. Sowers. Semiparametric regression for periodic longitudinal hormone data from multiple menstrual cycles. *Biometrics*, 56:31–39, 2000.

---

**Algorithm 1** Variational algorithm for the random lag model. The algorithm for the random intercept model replaces  $B_{q(\lambda_g)}$  with  $B_{q(\sigma_u^2)}$  and sets  $\mathcal{P}_g = I_{N/2 \times N/2}$ .  $\Delta \log[p(\mathbf{y}; q)]$  denotes the change in  $\log[p(\mathbf{y}; q)]$ .

---

**Require:**  $B_{q(\sigma^2)}, B_{q(\lambda_0)}, B_{q(\lambda_1)}, B_{q(\lambda_\gamma)}, B_{q(\lambda_g)} > 0$  and  $\epsilon > 0$ , small

**while**  $\Delta \log[p(\mathbf{y}; q)] > \epsilon$  **do**

**if** Crossover **then**

$$\Sigma_{q(\boldsymbol{\theta})} \leftarrow \left[ \frac{a_e + \frac{N}{2}}{B_{q(\sigma^2)}} \mathbf{C}'\mathbf{C} + \text{blockdiag} \left\{ (\sigma_b^2)^{-1} I_{p \times p}, \frac{a_0 + \frac{1}{2}K_0}{B_{q(\lambda_0)}} \mathcal{P}_0, \frac{a_1 + \frac{1}{2}K_1}{B_{q(\lambda_1)}} \mathcal{P}_1, \frac{a_g + \frac{1}{2}K_g}{B_{q(\lambda_g)}} \mathcal{P}_g \right\} \right]^{-1}$$

**else if** Longitudinal **then**

$$\Sigma_{q(\boldsymbol{\theta})} \leftarrow \left[ \frac{a_e + \frac{N}{2}}{B_{q(\sigma^2)}} \mathbf{C}'\mathbf{C} + \text{blockdiag} \left\{ (\sigma_b^2)^{-1} I_{p \times p}, \frac{a_\gamma + \frac{1}{2}K_\gamma}{B_{q(\lambda_\gamma)}} \mathcal{P}_\gamma, \frac{a_g + \frac{1}{2}K_g}{B_{q(\lambda_g)}} \mathcal{P}_g \right\} \right]^{-1}$$

**end if**

$$\boldsymbol{\mu}_{q(\boldsymbol{\theta})} \leftarrow \left( \frac{a_e + \frac{N}{2}}{B_{q(\sigma^2)}} \right) \Sigma_{q(\boldsymbol{\theta})} \mathbf{C}'\mathbf{Y}$$

$$B_{q(\sigma^2)} \leftarrow b_e + \frac{1}{2} \left[ \left\{ \mathbf{Y} - \mathbf{C}\boldsymbol{\mu}_{q(\boldsymbol{\theta})} \right\}' \left\{ \mathbf{Y} - \mathbf{C}\boldsymbol{\mu}_{q(\boldsymbol{\theta})} \right\} + \text{tr} \{ \mathbf{C}'\mathbf{C} \} \Sigma_{q(\boldsymbol{\theta})} \right]$$

**if** Crossover **then**

$$B_{q(\lambda_0)} \leftarrow b_0 + \frac{1}{2} \left[ \boldsymbol{\mu}_{q(\boldsymbol{\gamma}_0^S)}' \boldsymbol{\mu}_{q(\boldsymbol{\gamma}_0^S)} + \text{tr} \left\{ \frac{a_0 + \frac{1}{2}K_0}{B_{q(\sigma_0^2)}} \mathcal{P}_0 \right\} \right]$$

$$B_{q(\lambda_1)} \leftarrow b_1 + \frac{1}{2} \left[ \boldsymbol{\mu}_{q(\boldsymbol{\gamma}_1^S)}' \boldsymbol{\mu}_{q(\boldsymbol{\gamma}_1^S)} + \text{tr} \left\{ \frac{a_1 + \frac{1}{2}K_1}{B_{q(\sigma_1^2)}} \mathcal{P}_1 \right\} \right]$$

**else if** Longitudinal **then**

$$B_{q(\lambda_\gamma)} \leftarrow b_\gamma + \frac{1}{2} \left[ \boldsymbol{\mu}_{q(\boldsymbol{\gamma}_\gamma^S)}' \boldsymbol{\mu}_{q(\boldsymbol{\gamma}_\gamma^S)} + \text{tr} \left\{ \frac{a_\gamma + \frac{1}{2}K_\gamma}{B_{q(\sigma_\gamma^2)}} \mathcal{P}_\gamma \right\} \right]$$

**end if**

$$B_{q(\lambda_g)} \leftarrow b_g + \frac{1}{2} \left[ \boldsymbol{\mu}_{q(\boldsymbol{\gamma}_g^S)}' \boldsymbol{\mu}_{q(\boldsymbol{\gamma}_g^S)} + \text{tr} \left\{ \frac{a_g + \frac{1}{2}K_g}{B_{q(\sigma_g^2)}} \mathcal{P}_g \right\} \right]$$

**end while**

---

Table 1: Percent of simulated models correctly identified, by decision rule, for the crossover design when  $\ell = 60$ . Int. is short for intercept.

Effect	True Model	$n$	Decision Rule			
			min	< 2	< 5	< 10
Peak	Int.	25	97.88%	98.44%	98.98%	99.67%
		50	99.26%	99.67%	99.83%	99.95%
	Lag	25	100.0%	100.0%	100.0%	100.0%
		50	100.0%	100.0%	100.0%	100.0%
Cyclical	Int.	25	97.89%	98.51%	99.00%	99.80%
		50	100.0%	100.0%	100.0%	100.0%
	Lag	25	100.0%	100.0%	100.0%	100.0%
		50	100.0%	100.0%	100.0%	100.0%
Sigmoidal	Int.	25	98.14%	98.41%	98.97%	99.72%
		50	100.0%	100.0%	100.0%	100.0%
	Lag	25	100.0%	100.0%	100.0%	100.0%
		50	100.0%	100.0%	100.0%	100.0%

Table 2: Average absolute bias and MISE for the crossover design when  $\ell = 60$ . Int. is short for intercept.

Effect	True Model	$n$	Specified Model			
			Bias		MISE	
			Lag	Int.	Lag	Int.
Peak	Int.	25	0.1525	0.1298	0.0568	0.0391
		50	0.1053	0.0970	0.0215	0.0218
	Lag	25	0.4874	0.6187	0.4809	0.7840
		50	0.2223	0.4236	0.0822	0.3094
Cyclical	Int.	25	0.1108	0.0904	0.0247	0.0156
		50	0.0650	0.0485	0.0073	0.0041
	Lag	25	0.4741	0.6117	0.4542	0.7642
		50	0.2027	0.4137	0.0680	0.2904
Sigmoidal	Int.	25	0.1116	0.0909	0.0249	0.0157
		50	0.0653	0.0487	0.0074	0.0042
	Lag	25	0.4727	0.6107	0.4515	0.7621
		50	0.2026	0.4132	0.0679	0.2898

Table 3: Coverage by interval type for the crossover design when  $\ell = 60$ . Int. is short for intercept. All intervals were constructed at the 95% level.

Effect	True Model	$n$	Specified Model			
			Point-wise		Simultaneous	
			Lag	Int.	Lag	Int.
Peak	Int.	25	91.65%	90.61%	100.0%	100.0%
		50	88.80%	85.92%	100.0%	100.0%
	Lag	25	86.32%	95.36%	100.0%	100.0%
		50	91.84%	90.55%	100.0%	100.0%
Cyclical	Int.	25	93.90%	93.37%	100.0%	100.0%
		50	93.98%	93.83%	100.0%	100.0%
	Lag	25	86.52%	95.60%	100.0%	100.0%
		50	93.16%	91.12%	100.0%	100.0%
Sigmoidal	Int.	25	93.73%	93.21%	100.0%	100.0%
		50	93.81%	93.70%	100.0%	100.0%
	Lag	25	86.51%	95.58%	100.0%	100.0%
		50	93.18%	91.13%	100.0%	100.0%

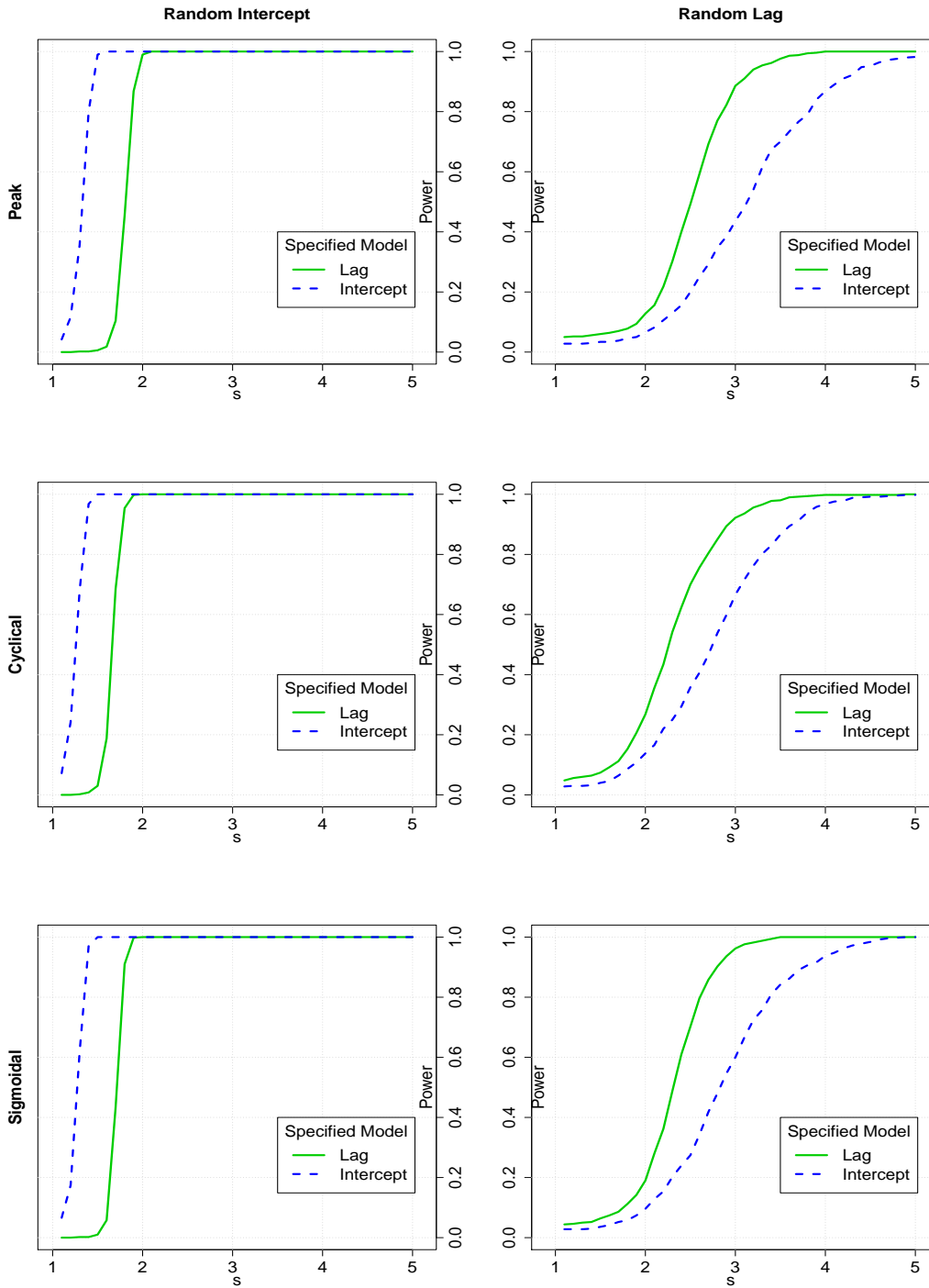


Figure 1: Power curves by true effect when  $\ell = 60$  and  $n = 25$ . Rows denote true effects, columns correspond to the true model. Solid green lines indicate a specified random lag model, dashed blue lines indicate a specified random intercept model. The x-axis,  $s$ , is the scaling factor dictating the difference in the curves.

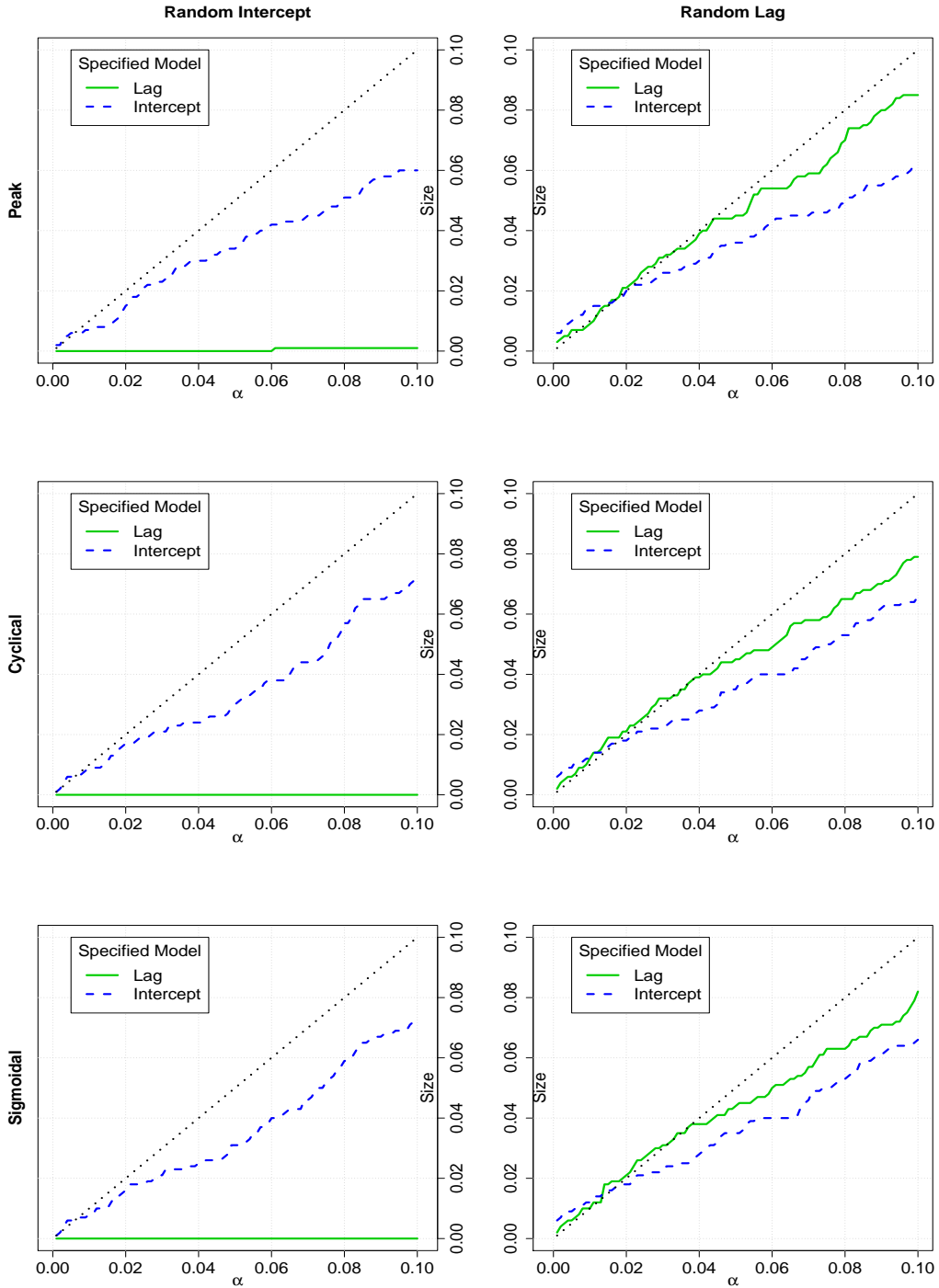


Figure 2: Size curves by true effect when  $\ell = 60$  and  $n = 25$ . Rows denote true effects, columns correspond to the true model. Solid green lines indicate a specified random lag model, dashed blue lines indicate a specified random intercept model. The x-axis is the  $\alpha$  level. The dotted black line denotes ‘nominal’ under each  $\alpha$ .



Table 4: VAICs for the random lag and random intercept (Int.) models for both outcomes and designs in the primary analysis. The ZLS  $p$ -value testing the difference in the curves between experimental conditions is included for the crossover models with the smallest VAIC by outcome.

Design	Outcome	Model	VAIC	ZLS Test		
				$\chi^2_\nu$	$\nu$	$p$ -value
Crossover	HR	Lag	466.7	—	—	—
		Int.	445.5	1.695	4.177	0.8126
	rMSSD	Lag	176.3	—	—	—
		Int.	155.9	0.679	3.616	0.9321
Longitudinal	HR	Lag	456.6	—	—	—
		Int.	433.5	—	—	—
	rMSSD	Lag	168.8	—	—	—
		Int.	139.9	—	—	—

Table 5: VAICs for the random lag and random intercept (Int.) models for both outcomes in the secondary analysis. The ZLS  $p$ -value testing the difference in the curves between experimental conditions is included for the model with the smallest VAIC by outcome and subgroup.

Group	Outcome	Model	VAIC	ZLS Test		
				$\chi^2_\nu$	$\nu$	$p$ -value
Healthy	HR	Lag	57.59	3.740	3.503	0.3666
		Int.	59.53	—	—	—
	rMSSD	Lag	48.44	—	—	—
		Int.	38.29	0.669	1.663	0.6305
Cardiac	HR	Lag	49.41	—	—	—
		Int.	49.34	8.473	2.090	0.0160
	rMSSD	Lag	45.76	—	—	—
		Int.	34.23	0.572	3.122	0.9142
Smoker	HR	Lag	108.9	0.786	1.732	0.6070
		Int.	232.7	—	—	—
	rMSSD	Lag	74.98	3.245	4.866	0.6444
		Int.	83.49	—	—	—